GENETICS

Requirement of WDR70 for POLE3-mediated DNA double-strand breaks repair

Xiaobing Mao[1], Jian Wu[1], Qin Zhang[1], Su Zhang[1], Xiaoshuang Chen[1], Xueqin Liu[1], Mingtian Wei[2], Xiaowen Wan[1], Lei Qiu[1], Ming Zeng[3], Xue Lei[1], Cong Liu[3], Junhong Han[1]*

H2BK120ub1 triggers several prominent downstream histone modification pathways and changes in chromatin structure, therefore involving it into multiple critical cellular processes including DNA transcription and DNA damage repair. Although it has been reported that H2BK120ub1 is mediated by RNF20/40 and CRL4^{WDR70}, less is known about the underlying regulation mechanism for H2BK120ub1 by WDR70. By using a series of biochemical and cell-based studies, we find that WDR70 promotes H2BK120ub1 by interacting with RNF20/40 complex, and deposition of H2BK120ub1 and H3K79me2 in *POLE3* loci is highly sensitive to *POLE3* transcription. Moreover, we demonstrate that POLE3 interacts CHRAC1 to promote DNA repair by regulation on the expression of homology-directed repair proteins and KU80 recruitment and identify CHRAC1 D121Y mutation in colorectal cancer, which leads to the defect in DNA repair due to attenuated the interaction with POLE3. These findings highlight a previously unknown role for WDR70 in maintenance of genomic stability and imply POLE3 and CHRAC1 as potential therapeutic targets in cancer.

INTRODUCTION

Genomic instability is a hallmark of cancer (*1*, *2*). Rapid and efficient repair of DNA damage helps to maintain genomic integrity, which is critical for cell survival and viability. In contrast, dysfunctional DNA damage response (DDR) leads to unrepaired DNA damage disrupting genomic integrity, which induces various aberrant cellular behaviors. The DNA double-strand break (DSB), one of the most powerful activators, can be repaired via homologous recombination (HR) or nonhomologous end-joining (NHEJ) pathway (*3*, *4*). Although different DNA repair pathways have different components, there are several common characteristics in response to DNA damage. In brief, DNA damage sensors are immediately recruited to the DNA damage site, which serve as a platform to recruit the mediators. HR usually exists in S phase or G_2 phase without error in DNA damage repair because it is required homologous sequence as a template. HR is initiated by recruitment of MRN complex to degrade nucleolytic from 5′ to 3′ in combination with the C-terminal binding protein (CtBP) interacting protein (CtIP), generating a 3′ single-strand DNA (ssDNA) (*5*). Replication protein A (RPA) complex, which is composed of RPA1, RPA2, and RPA3, binds to the naked ssDNA to protect it. Subsequently, RPA complex is replaced with RAD51 recombinase immediately, which is important for chromosome synapsis and sister chromatid exchange (*6*). However, the process of classic NHEJ is not as complicated as the HR. KU70 and KU80 forms a complex at broken site to activate DNA–protein kinase C (DNA-PKc) recruiting DNA ligase IV for re-ligating the broken DNA independent on homologous sequence (*7*). Therefore, NHEJ can be performed in the any phase while it is error prone.

The monoubiquitylation of H2B lysine residue 120 (H2BK120ub1) is one of the most marked chromatin modifications. H2BK120ub1 functions as a signaling hub to trigger several prominent downstream histone modification pathways and to decompact chromatin structure, therefore involving it into multiple critical cellular processes, including DNA transcription, DNA damage repair, and DNA replication (*8*–*16*). For example, the positive cross-talk between H2BK120ub1 and H3K79me2 has been reported previously; in particular, H2BK120ub1 is a prerequisite for histone H3K4me3 and H3K79me2, two known active transcription markers (*8*, *15*, *17*–*19*). In addition to H2B ubiquitylation at lysine-120 by breast cancer gene 1 (BRAC1) and mouse double minute 2 (MDM2), the heterodimer E3 ligase Ring finger protein 20/40 (RNF20/40) also monoubiquitylates H2B at lysine-120, and a previous study has proposed that the phosphorylation of RNF20 serine-172 by ataxia telangiectasia mutated (ATM) kinase can facilitate HR and NHEJ (*12*). WD repeat–containing protein 70 (WDR70), which is composed of six WD40 repeat domain functions as a subunit of CRL4 complex in homology-directed repair (HDR) by regulating the transcription of *BRCA1*, *BRCA2*, *RAD51*, and substantial additional transcriptomic changes (*20*). CRL4^{WDR70} could promote the monoubiquitylation of H2B to affect DNA resection and thus HDR (*21*). Despite all these, our current understanding of the factors that regulate H2BK120ub1 in DDR need to be further polished.

Here, we show that WDR70 interacts with RNF20/40 to facilitate H2BK120 monoubiquitylation and functions in DDR. We define the mechanistic basis of WDR70 binding to RNF20/40 and uncover an intrinsic ubiquitylation activity toward H2BK120 in coordination with RNF20/40. Depletion of WDR70 directly affects on genomic integrity by interrupting HR and NHEJ. Furthermore, DNA polymerase epsilon 3 (POLE3) expression is enhanced in WDR70-RNF20/40 apparatus–dependent manner. The direct interaction between POLE3 and CHRAC1, a component of chromatin accessibility complex (CHRAC) (*22*, *23*), is also observed to promote DNA repair by regulation on the expression of HDR

[1]Department of Biotherapy, Cancer Center and State Laboratory of Biotherapy, and Frontiers Science Center for Disease-related Molecular Network, West China Hospital, Sichuan University, Chengdu 610041, China. [2]Department of Gastrointestinal Surgery, West China Hospital, Sichuan University, Chengdu 610041, China. [3]Department of Pediatrics, Key Laboratory of Birth Defects and Related Diseases of Women and Children (Ministry of Education), West China Second University hospital, Sichuan University, Chengdu 610041, China.
*Corresponding author. Email: hjunhong@scu.edu.cn

proteins and KU80 recruitment. We further identify CHRAC1 D121Y mutation in colorectal cancer (CRC) and observe that this mutation leads to the defect in DNA repair due to attenuated the interaction with POLE3. Collectively, our work reveals an important role of WDR70 in chromatin integrity maintenance.

RESULTS

WDR70 associates with H2B ubiquitylation E3 ligase RNF20/40

To screen proteins associating with WDR70, the affinity purification coupled mass spectrometry was conducted in human embryonic kidney (HEK) 293T cells. The ectopically expressed hemagglutinin (HA)–WDR70 in HEK293T was immunoprecipitated using anti-HA antibody–coated magnetic beads. Intriguingly, H2BK120ub1 E3 ligase RNF20 and RNF40 were coimmunoprecipitated with WDR70 (Fig. 1A). In addition to RNF20/40, DNA damage-binding protein 1 (DDB1) and Exportin 1 (XPO1) also appeared in the target list of the mass spectrometry data. In addition to RNF20/40, DDB1, which has been identified as a critical player in DDR, and XPO1, an important carrier for TP53 and BRCA1 (both are critical for DDR), were validated in WDR70 coimmunoprecipitated fraction as well (Fig. 1B). In addition, the interaction between WDR70 and RNF20/40 was further confirmed using specific antibody against N terminus of WDR70 in HCT116 and HT29 colorectal cancer cells (Fig. 1, C and D). Moreover, WDR70-RNF20/40 interaction was validated in HEK293T cells cotransfected with HA-WDR70 with either MYC-RNF20 or MYC-RNF40 plasmids (Fig. 1, E and F). Collectively, these experiments provide evidence that WDR70 interacts with RNF20/40. To test the effect of WDR70 on H2K120ub1 expression, we knocked down WDR70 and investigated H2K120ub1 level in cells. H2K120ub1 was notably reduced in cells lacking WDR70, consistent with the result of RNF20/40 silencing (Fig. 1G). In line with a previous discovery (*12*), we also observed the dependence of the stability of RNF20 and RNF40 on their interaction with each other but little on WDR70 (Fig. 1G). Together, these results support the idea that WDR70-RNF20/40 apparatus is critical for de novo H2K120 monoubiquitylation.

WD40 domains of WDR70 are required for association with RNF20/40 and H2BK120 ubiquitylation

To further understand the importance of our findings in a cellular context, we elected to focus on mapping the regions of WDR70 involved in the interaction with RNF20/40. A series of WDR70 truncation mutants were constructed, and HEK293T cells were transiently cotransfected cells with a series of HA-tagged *WDR70* mutants and MYC-tagged *RNF20* or *RNF40* plasmids (Fig. 2A). The cell lysates from these cells were subjected to immunoprecipitation using specific antibody against MYC tag, and the levels of WDR70, RNF20, and RNF40 therein were analyzed by Western blotting. Gratifyingly, we observed a remarkable reduction of WDR70 in mutants that lack two coiled-coil domains at the N terminus of WDR70 (Fig. 2B), suggesting that these two coiled-coil domains substantially contribute to WDR70-RNF20/40 interaction. In addition, deleting either of single WD40 domain in WDR70 slightly weakened the interactions between WDR70 and RNF20, whereas loss of entire WD40 domains (D10 mutant) completely abolished the interaction (Fig. 2B). Similar results were also obtained in RNF40 immunoprecipitation assay, although loss of either one single WD40 domain had a little alteration in the interaction between WDR70 and RNF40 (Fig. 2C). These results imply that the majority of interaction is attributed to entire WD40 domains of WDR70, albeit the coiled-coil domains at N terminus help the stability of WDR70-RNF20/40 interaction.

The interaction observed between WDR70 and RNF20/40 prompted us to ask whether WDR70 plays a role as molecular chaperones like WW domain containing adapter with coiled-cell (WAC) protein, which interacts with the RNA polymerase II transcriptional machinery via its WW domain and with RNF20/40 via its coiled-coil region, thereby linking and regulating H2BK120ub1 (*24*). We knocked down WDR70 in HEK293T cells coexpressing RNF20 and RNF40 to investigate the stability of RNF20-RNF40 complex and observed no obvious alteration in cells lacking WDR70 or resupplying WDR70 (Fig. 2D). It is worth stressing that WDR70 contains six WD40 domains and WD40 domain could serve as a previously unidentified ubiquitin-interaction domain (*25*). Thus, we speculated that WDR70 may serve as the ubiquitin reservoir for H2BK120ub1 by RNF20/40. To test this possibility, we cotransfected HEK293T cells with Flag-ubiquitin and wild-type or entire WD40 domains deletion of WDR70 and detected WDR70 ubiquitylation by immunoblot. In contrast to loss of WD40 domains, strong signal of WDR70 ubiquitylation was detected, suggesting that WD40 domains of WDR70 are involved in ubiquitylation (Fig. 2, E and F). However, it is unclear whether WD40 domains of WDR70 contribute to the steady levels of H2BK120ub1. In contrast to ectopic expression of wild-type WDR70, WD40 domains deletion mutant failed to restore H2BK120ub1 modification in cells lacking endogenous WDR70 (Fig. 2, G and H). Intriguingly, ectopically expressing either RNF20 or RNF40 was not able to recover H2BK120ub1 modification in cells lacking WDR70 (Fig. 2, G and H). Collectively, these experiments indicate that WDR70 and in particular WD40 domains contributes substantially to the interaction with RNF20/40 and de novo H2BK120ub1.

WDR70 knockdown induces genomic instability by suppressing DDR

H2BK120ub1 predominantly catalyzed by RNF20/40 inhibits 53BP1-mediated DNA damage signaling and is required for timely DNA strand break repair (*26*), and loss of H2BK120ub1 was frequently detected in tumors (*27*, *28*). During double-strand DNA break repair, RNF20 is phosphorylated by ATM, and loss of RNF20 impairs HR repair and NHEJ (*12*, *29*), and ssDNA binding factor RPA complex functions as a master regulator by coupling H2BK120ub1 to DNA repair for the spatial-temporal control recombination (*30*). Thus, we next moved to validation of the most interesting event about WDR70 involvement in the maintenance of genomic stability. To this end, we treated HCT116 or HT29 cells with camptothecin (CPT) to induce DNA damage and observed remarkable reduction of γH2AX and phosphorylated RPA2 (p-RPA2/p-RPA32) foci in cells lacking WDR70 (Fig. 3, A and B, and fig. S1, A and B). Moreover, WDR70 knockdown also remarkably attenuated the phosphorylation of ATR, CHK1, H2A (herein, γH2AX), and RPA2, which is known as an important event to initiate DDR, detected by Western blotting (Fig. 3C). Together, these results imply an impaired DDR in cells lacking WDR70 expression and suggest the significance of WDR70 in the maintenance of genomic stability, and this notion was further supported by the result of comet assay, which showed longer tails

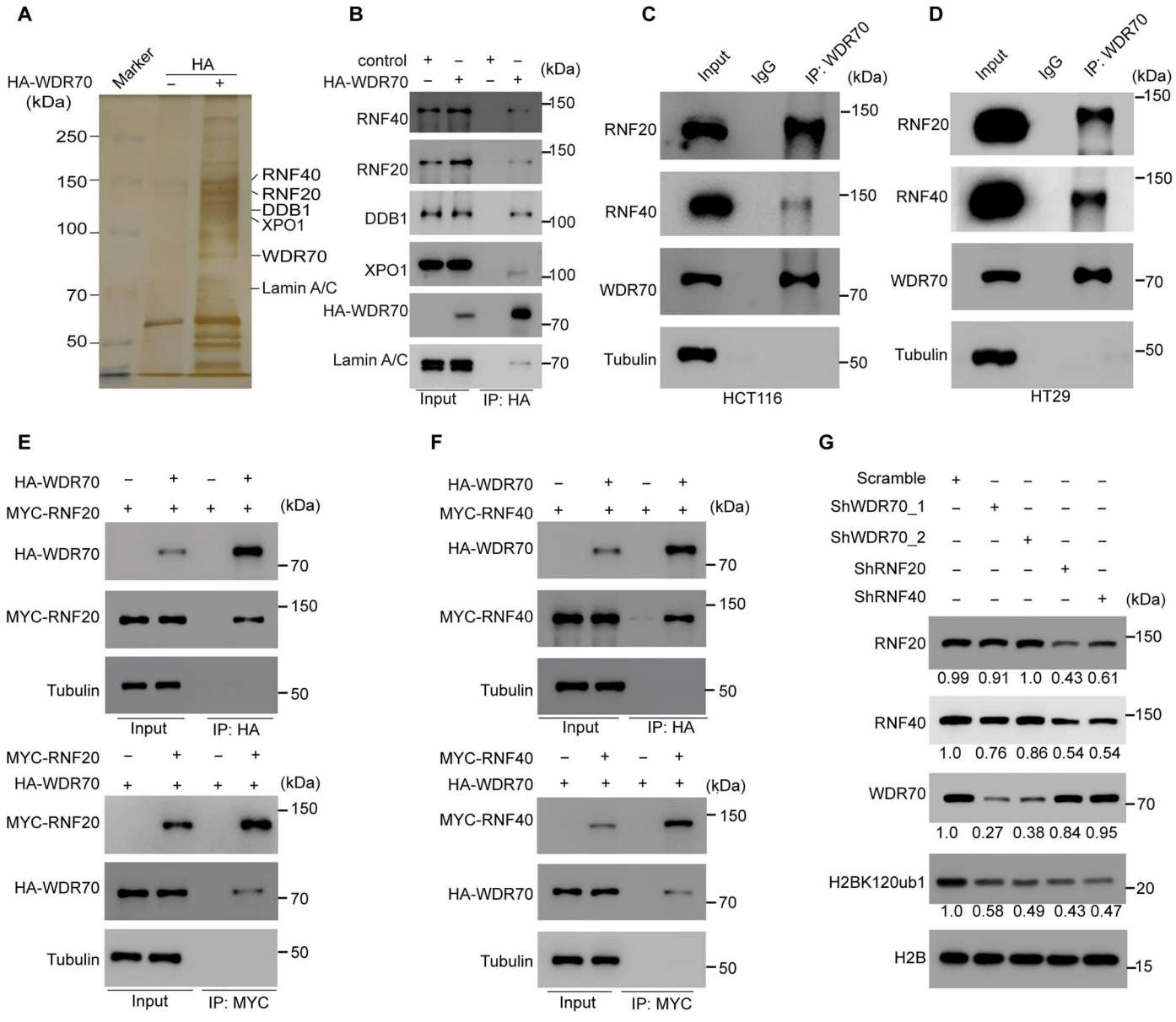

Fig. 1. WDR70 interacts with RNF20/40 complex in vivo. (**A**) Silver staining showing affinity capture of proteins from HEK293T cells stably expressing HA-WDR70 by immunoprecipitation (IP) with anti-HA magnetic beads. Putative RNF20 and RNF40 were indicated and confirmed by mass spectrometry analysis. (**B**) Coimmunoprecipitation with HA-WDR70 by capturing of proteins from HEK293T cells stably expressing HA-WDR70 and Western blot analysis for indicated proteins. (**C** and **D**) Coimmunoprecipitation of endogenous RNF20 and RNF40 with WDR70 in HCT116 (C) or HT29 cells (D). After immunoprecipitation with anti-WDR70 antibody, immunoblots were performed with the indicated antibodies. IgG, immunoglobulin G. (**E**) Coimmunoprecipitation of RNF20 with WDR70. Whole-cell extracts of HEK293T cells cotransfected with *HA-WDR70* and *MYC-RNF20* were applied to anti-HA or anti-MYC magnetic beads. After extensive washing the bead, captured proteins were detected by Western blotting using specific antibodies as indicated. (**F**) Coimmunoprecipitation of WDR70 with RNF40. Whole-cell extracts of HEK293T cells cotransfected with *HA-WDR70* and *MYC-RNF40* applied to anti-HA or anti-MYC magnetic beads. After extensive washing beads, captured proteins were detected by Western blotting using specific antibodies as indicated. (**G**) Detection of H2BK120ub1 modification levels in shWDR70, shRNF20, or shRNF40 HCT116 cells by Western blotting. Quantification of protein band intensity by ImageJ software. The indicated H2BK120ub1 level was normalized to the total H2B expression, while other proteins were normalized to its expression in the scramble group.

(Fig. 3D and fig. S1, C and D), and by increased micronuclei frequency (fig. S1, E and F) and by the result of cytogenetic analysis, which showed a notable increase of aberrant chromosomes, including broken, fusion, and fragmentation when WDR70 was knocked down (Fig. 3E and fig. S1, G and H). HR and NHEJ are two major pathways to repair the DSBs in DNA. Loss-of-function or deleterious mutations in HR or NHEJ genes contribute to repair deficiency. We also found that loss of WDR70 trimmed the frequency of HR and NHEJ by approximately 50% in cells (Fig. 3, F and G). Rapid and efficient repair of DNA damage helps to maintain genomic integrity, which is critical for cell survival and viability. In contrast, dysfunctional DDR leads to unrepaired DNA damage

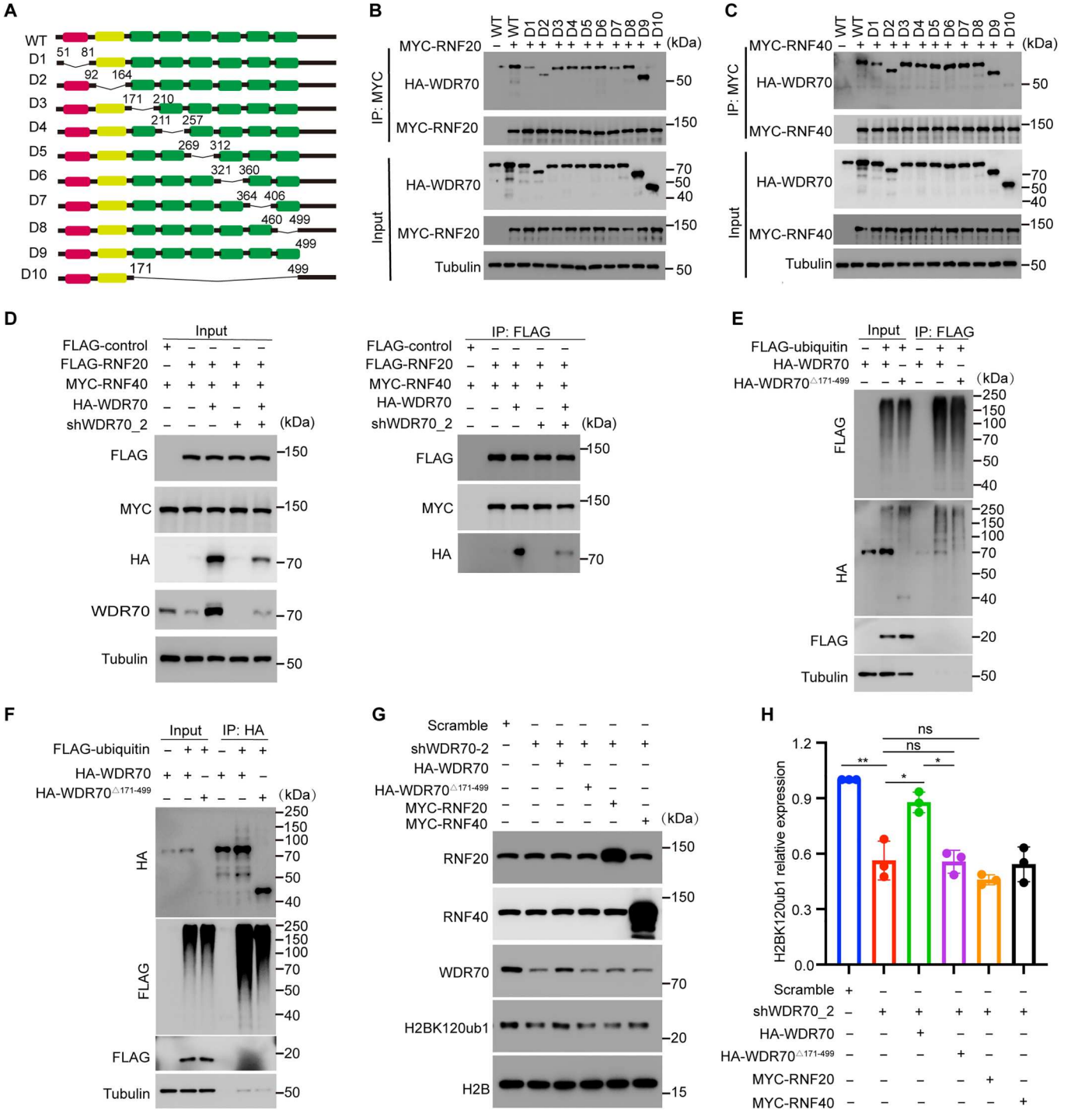

Fig. 2. Mapping the regions of WDR70 associating with RNF20/40. (**A**) Schematic diagram of wild-type and truncated WDR70 used in the study. (**B** and **C**) Coimmunoprecipitation of wild-type and truncated WDR70 with RNF20 or RNF40. Whole-cell extracts of HEK293T cells cotransfected with *HA-WDR70* and *MYC-RNF20* (B) or *MYC-RNF40* (C) applied to anti-MYC magnetic beads. Captured proteins were detected by Western blotting using specific antibodies as indicated. (**D**) The stability of RNF20/40 complex. Detection of RNF20 and RNF40 expression in HEK293T cells knocking down WDR70 by shRNA with or without ectopic expression of HA-WDR70 (left). RNF20-RNF40 complex was detected by coimmunoprecipitated using anti-FLAG antibody in WDR70 knockdown cells with or without ectopic expression of HA-WDR70 (right). (**E** and **F**) Loss of WD40 domains (D10) reduced WDR70 ubiquitylation in vivo. Immunoprecipitation of FLAG (E) or HA (F) in HEK293T cells cotransfected with FLAG-ubiquitin and wild-type or WD40 domain deletion HA-WDR70 (D10). The resulted proteins were detected by Western blotting using specific antibodies as indicated. (**G** and **H**) Detection of H2BK120ub1 modification levels by Western blotting in shWDR70 cells with or without ectopic expression of RNF20 or RNF40. Whole-cell extracts from WDR70 knockdown cells cotransfected with *HA-WDR70* and *MYC-RNF20* or *MYC-RNF40* were subjected to SDS–polyacrylamide gel electrophoresis (PAGE) followed by Western blotting (G). Quantification of H2BK120ub1 band intensity by ImageJ software (H). The indicated H2BK120ub1 level was normalized to the total H2B expression. Error bars represent mean ± SD from at least three independent experiments. *P < 0.05 and **P < 0.01. ns, not significant.

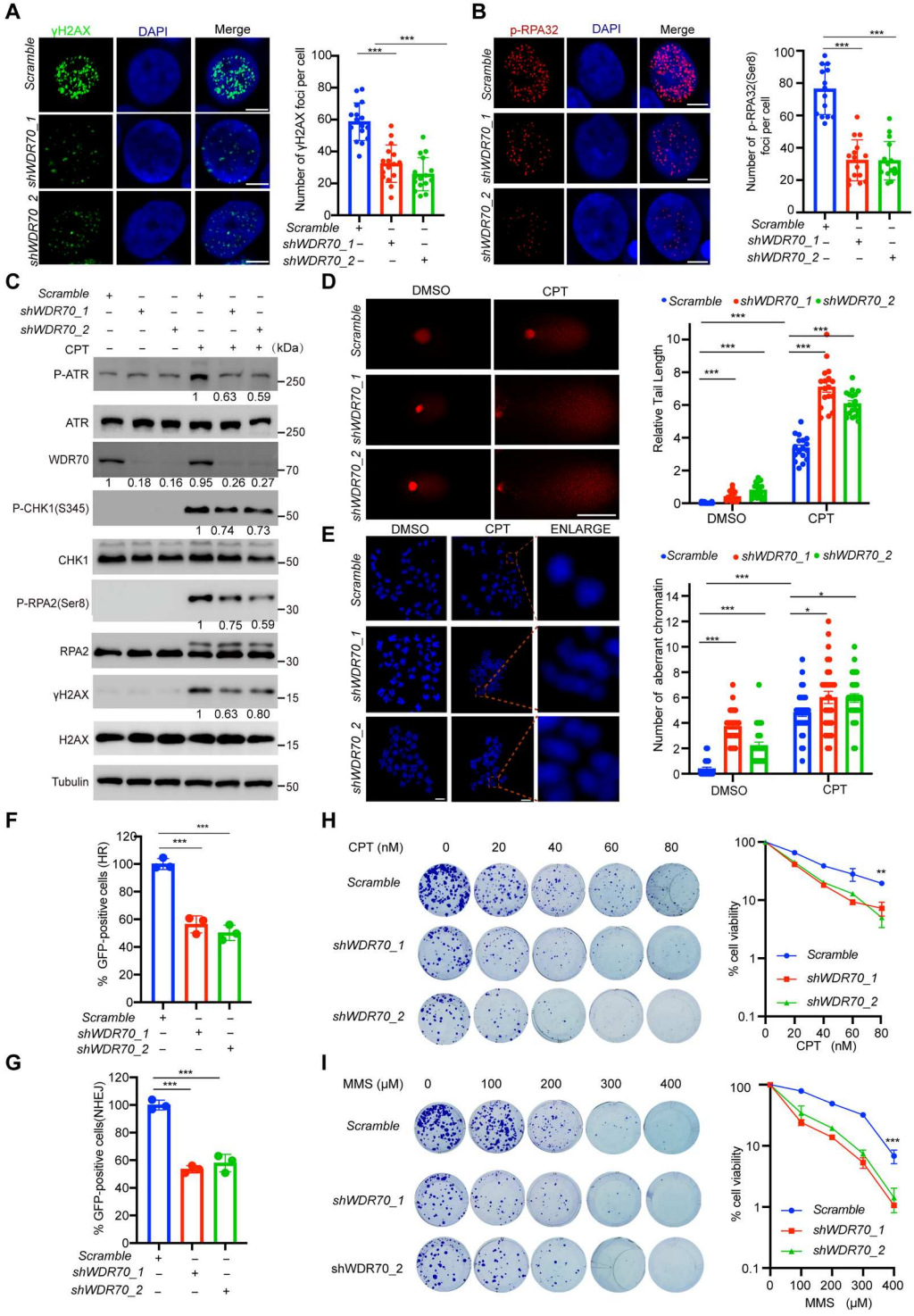

Fig. 3. WDR70 is required for genome integrity. (**A** and **B**) Representative images of γH2AX foci (A), phosphorylated RPA2 (p-RPA32) foci (B), and 4′,6-diamidino-2-phenylindole (DAPI)–stained nuclei in control or shWDR70 HCT116 cells treated with CPT for 4 hours. Scale bars, 5 μm. Quantification of γH2AX foci per cell and p-RPA32 foci per cell (right). The number from three independent experiments is shown. (**C**) Western blotting analysis showing the indicated proteins associated with DDR in HCT116 cells under the same conditions as (A). (**D**) Direct observation of DNA damage by using the comet assay in HCT116 cells after CPT treatment for 12 hours. Representative images are shown. Scale bar, 50 μm. Quantitation of the comet data (right). The length and intensity of DNA tails relative to heads is shown as % of the relative comet tail moment. DMSO, dimethyl sulfoxide. (**E**) Representative images of aberrant chromosomes. HCT116 cells with or without WDR70 knockdown was treated with CPT followed by karyotype assay. Scale bars, 5 μm. Quantitation of aberrant chromosomes per cell (right). Total 30 cells were counted in each group. (**F** and **G**) HR (F) and NHEJ (G) efficiency assay for chromosomal DSB induced by endonuclease I-Sce I. GFP-positive cell fraction in DR-GFP U2OS cells (F) and in EJ5-GFP U2OS cells (G). The efficiency of HR and NHEJ was determined in WDR70-deficient cells by fluorescence-activated cell sorting (FACS)–based fluorescence readout. The results are shown as mean ± SD (n = 3). (**H** and **I**) Representative images of colony formation (left) and survival curves (right). Cell viability based on clonogenic growth of HCT116 cells transfected with scramble shRNA or shWDR70 plasmid in the presence of CPT (L) or Methyl methanesulfonate (MMS) (M) for 24 hours. Error bars represent SD. *P < 0.05, **P < 0.01, and ***P < 0.001.

disrupting genomic integrity, which induces various aberrant cellular behaviors. We observed obvious reduction of cell viability in response to the treatment of CPT or methyl methanesulfonate (MMS), one of classical DNA-damaging agents, when WDR70 was knocked down (Fig. 3, H and I, and fig. S1, I and J). These results further strengthen the notion about the critical role of WDR70 in maintaining genomic stability.

POLE3 is a potential target of WDR70

To further screen genes regulated by WDR70, the total RNA was extracted for RNA sequencing in cells with suppression of WDR70 using short hairpin RNA (shRNA). Inspection of the transcriptome data revealed that total 418 genes is predominantly affected by WDR70 knockdown, including up-regulated 206 genes and down-regulated 212 genes (Fig. 4A). Specifically, down-regulated

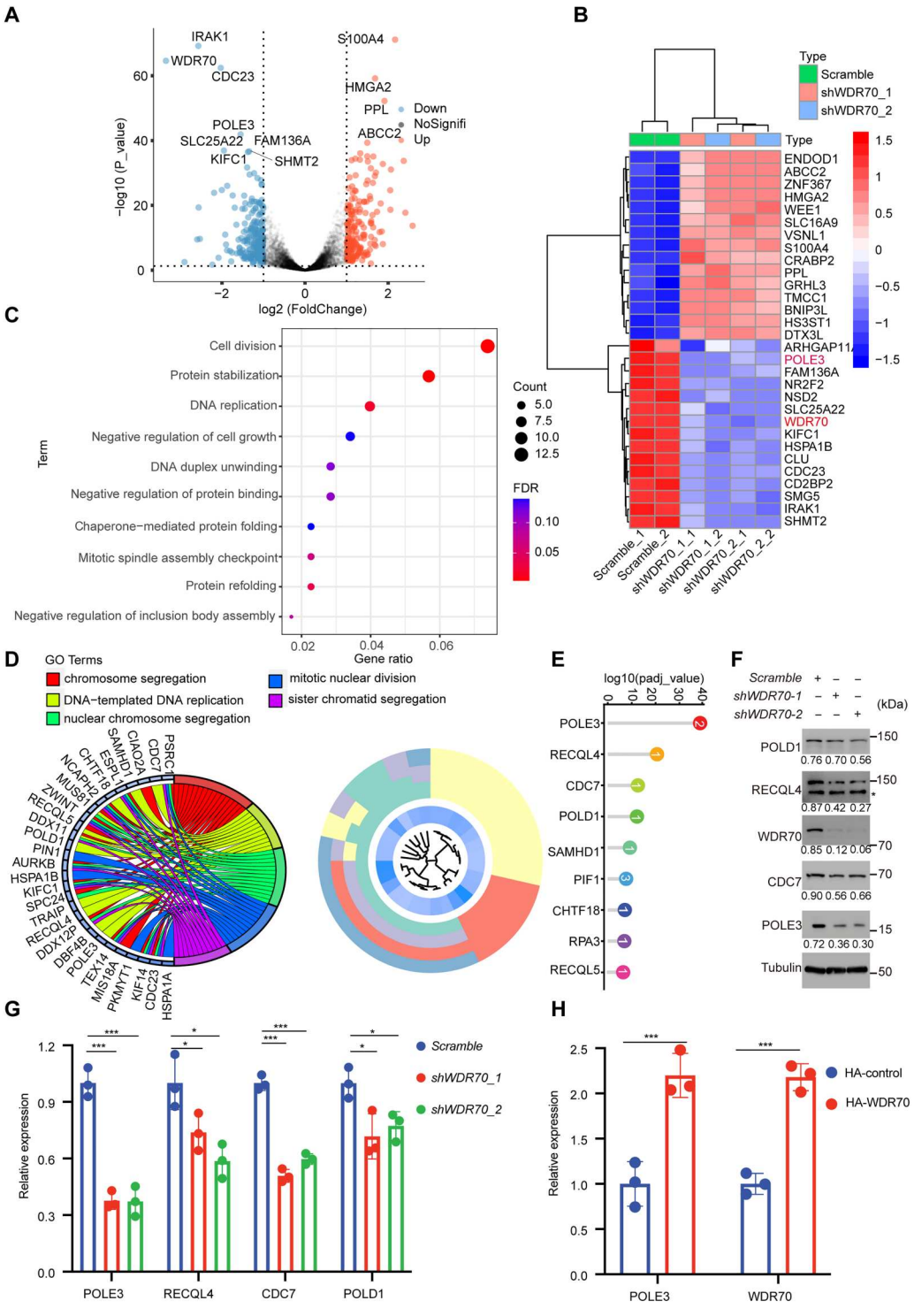

Fig. 4. WDR70 suppresses POLE3 expression. (**A** and **B**) The volcano plots (A) and heatmap (B) of differentially expressed genes including POLE3 in WDR70 knockdown HCT116 cells. The relative expression of genes with log2 (fold change) beyond 1 or below 1 with adjusted *P* value lower than 0.05 were considered as significantly differential expression. (**C**) The enriched GO biological process was shown in bubble plot. *x* axis represents GeneRatio whereas *y* axis is biological process. (**D**) The analysis of five enriched GO annotations from the DAVID GO terms, including GO CC, GO BP, and GO MF were displayed using circus plots. Colored ribbons represented different GO terms. The line with different color connects genes involvement in the GO terms. (**E**) The enriched genes in DNA replication were shown in lollipop plot. *x* axis stands for the adjusted *P* value, whereas *y* axis indicates the gene. (**F** and **G**) Validation of the indicated gene expression using Western blotting (F) and qRT-PCR (G) in HCT116 cells knocking down WDR70. The indicated protein level was normalized to the tubulin expression and the quantification number was labeled below the protein bands (F). * in (F) indicates nonspecific protein bands. (**H**) Detection of POLE3 expression in HCT116 cells ectopically expressing WDR70 using qRT-PCR. The results are shown as mean ± SD normalized to actin ($n = 3$) (G and H). $^*P < 0.05$, $^{**}P < 0.01$, and $^{***}P < 0.001$.

genes are enriched in protein stabilization, DNA replication, and cell division (Fig. 4, B and C). By gene ontology (GO) analysis, the alteration of DNA replication, chromosome segregation, and sister chromatid segregation were found (Fig. 4D). It is known that H2BK120ub1 promotes gene transcription and elongation by altering the chromatin structure (*11*, *31*, *32*). Thus, transcription down-regulation by WDR70 knockdown may attribute to loss of H2BK120ub1. Among the down-regulated genes, genes associated with DNA replication including *POLE3*, a subunit of DNA polymerase epsilon, attracted our attention since CPT could induce DNA replication stress (Fig. 4, B and E). Consistent with our library data, the inhibitory effect on expression and transcription of *POLE3* was validated in WDR70 knockdown cells using immunoblot and quantitative real-time polymerase chain reaction (PCR;

Fig. 4, F and G). Conversely, ectopic expression of WDR70 notably increased *POLE3* transcription (Fig. 4H). It has been reported that POLE3 promotes checkpoint activation, and loss of POLE3 enhances cells′ sensitivity to ATR inhibitor, poly(adenosine 5′-diphosphate–ribose) polymerase (PARP) inhibitor, and CPT (*33*–*35*). Together, these results indicate that POLE3 is a potential target of WDR70, implying that POLE3 is probably involved in genomic integrity maintenance by WDR70.

Involvement of POLE3 in WDR70-mediated genomic integrity maintenance

POLE3, together with POLE4, forms a previously unidentified histone H3-H4 chaperone complex, which participates in the maintenance of chromatin integrity during DNA replication (*36*). Our results indicate that POLE3 is one of WDR70 targets and may be implicated in WDR70-mediated maintenance of genomic integrity. To validate this possibility further functionally, we knocked down POLE3 in HCT116, HT29, and HEK293T cells and found that loss of POLE3 also substantially decreased the foci formation of γH2AX and p-RPA2 after CPT treatment, which is consistent with the finding in cells lacking WDR70 (Fig. 5, A and B, and fig. S2, A and B). In addition, we observed obvious reduction in the expression of γH2AX, p-RPA2, and phosphorylated CHK1 in POLE3-deficient cells (Fig. 5C), longer comet tails, increased micronuclei and aberrant chromosomes, and enhanced sensitivity to CPT as well (Fig. 5, D to F, and fig. S2, C to J). Moreover, the frequency of HR and NHEJ was remarkably attenuated in cells lacking POLE3 (Fig. 5G). Together, these results indicate that POLE3 participate in the maintenance of chromatin integrity under the replication stress caused by CPT. Ectopic expression of POLE3 shortened comet tails and partially rescued HR and NHEJ from the defect caused by WDR70 deficiency (Fig. 5, H to J), implying the involvement of POLE3 in WDR70-mediated genomic integrity maintenance.

POLE3 promotes the recruitment of KU80 at DSBs sites in combination with CHRAC1

The CHRAC, which is composed of ATP-dependent chromatin assembly factor 1 (ACF1), SWI/SNF-related matrix-associated actin-dependent regulator of chromatin subfamily A member 5 (SMARCA5), POLE3, and CHRAC1, is assembled at DNA damage sites (*37*, *38*). Among the components of CHRAC, ACF1 can interact directly with the NHEJ protein KU70 and is required for the accumulation of KU70/80 complex at DNA DSBs (*38*). A recent study has found that budding yeast Dpb4 (POLE3 in mammals) plays two functions in sensing and processing DSBs. One of functions is that promoting histone removal and DSB resection by interacting with histone fold protein Dls1. The other is to promote checkpoint activation by interacting with Dpb3 (*35*). To assess the possible role of POLE3 in CHRAC complex during DSBs repair, we first used coimmunoprecipitation and fluorescence resonance energy transfer (FRET) assay to investigate the interaction with the subunits of CHRAC complex. CHRAC1, but not ACF1 and SMARCA5, was coimmunoprecipitated with POLE3 in HCT116 or HT29 Cells treated with CPT (Fig. 6, A and B, and fig. S3, A and B). In agreement with our coimmunoprecipitation results, the interaction between POLE3 and CHRAC1 was validated by FRET assay (Fig. 6C). To further characterize this interaction, we mapped the domains of POLE3 and CHRAC1 involved in the interaction and found that 85 to 124 amino acid residues in POLE3 are required for binding to CHRAC1 (Fig. 6D). In addition, we observed that CHRAC1 could coimmunoprecipitate with POLE3 using specific antibody against green fluorescent protein (GFP) tagged with CHRAC1, and 1 to 90 amino acid residues in CHRAC1 are essential for POLE3 association (Fig. 6E).

We next moved to investigate how POLE3-CHRAC1 complex functions in DSBs repair. Inspection of protein-protein interaction (PPI) database (BioGRID) revealed that 20 proteins concurrently appeared in both PPI network of POLE3 and CHRAC1 (Fig. 6F). Among these 20 proteins, we focused on KU80 protein encoded by *XRCC5* gene, which plays a critical role in NHEJ by forming KU70/80 complex (Fig. 6G). By coimmunoprecipitation assay, we validated the interaction between POLE3-CHRAC1 and KU80 in vivo and found that CPT treatment enhanced the interaction of POLE3 with KU80 (Fig. 6, H to I). Meanwhile, POLE3 knockdown obviously attenuated KU80 recruitment at DSBs sites produced by laser microirradiation (Fig. 6, J and K). Together, besides two known functions of POLE3 in DSBs repair, these results suggest that POLE3 also facilitate DSBs repair by recruiting or constraining KU70/80 complex at damage sites.

WDR70 regulates POLE3 expression in H2BK120ub1- and H3K79me2-dependent manner

Several histone marks including H2BK120ub1, H3K4me3, and H3K79me2 have been linked to active transcription (*39*, *40*). The positive cross-talk between H2BK120ub1 and H3K79me2 has been reported previously; in particular, H2BK120ub1 is a prerequisite for histone H3K4 and H3K79 methylation (*8*, *17*). In an attempt to define the underlying mechanism for regulation of POLE3 expression by WDR70, we conducted chromatin immunoprecipitation (ChIP) using specific antibodies against H2BK120ub1, H3K4me3, and H3K79me2 in HCT116 cells lacking WDR70. Notably, the significant reduction of H2BK120ub1 and H3K79me2 enrichment in *POLE3* promoter and coding region was found in WDR70-deficient cells, whereas it had little impact on H3K4me3 enrichment (Fig. 7A). By Western blot, we also confirmed the obvious reduction of POLE3 expression in cells with WDR70 knockdown (Fig. 7B). Considering WDR70 contribution to H2BK120ub1, these results imply that WDR70 promotes POLE3 expression by enhancing the enrichment of H2BK120ub1 and H3K79me2 in *POLE3* loci. To further validate this possibility, we transfected HCT116 cells either with the plasmids of FLAG-H2B or FLAG-H2B2KR (K120R K125R and H2B2KR), which can mimic H2B deubiquitylation (*41*), and found that H2B2KR failed to promote the expression of POLE3 and H3K79me2 (Fig. 7, C and D). Furthermore, both knocking down H3K79me2 DOT1 like histone lysine methyltransferase (DOT1L) and inhibiting DOT1L activity with EPZ004777 notably decreased POLE3 expression (Fig. 7, E to H). Given the role of H2BK120ub1 in regulating DNA repair, we also evaluated DOT1L contribution to DNA repair. As shown in fig. S4A, the phosphorylation of H2A and RPA2 was remarkably reduced in DOT1L-deficient cells. In addition, longer comet tails were also observed in cells lacking DOT1L (fig. S4, B and C). These data reveal that DOT1L is involved in DDR. Together, the above data indicate that WDR70 directly regulates POLE3 expression in H2BK120ub1 and H3K79me2-dependent manner.

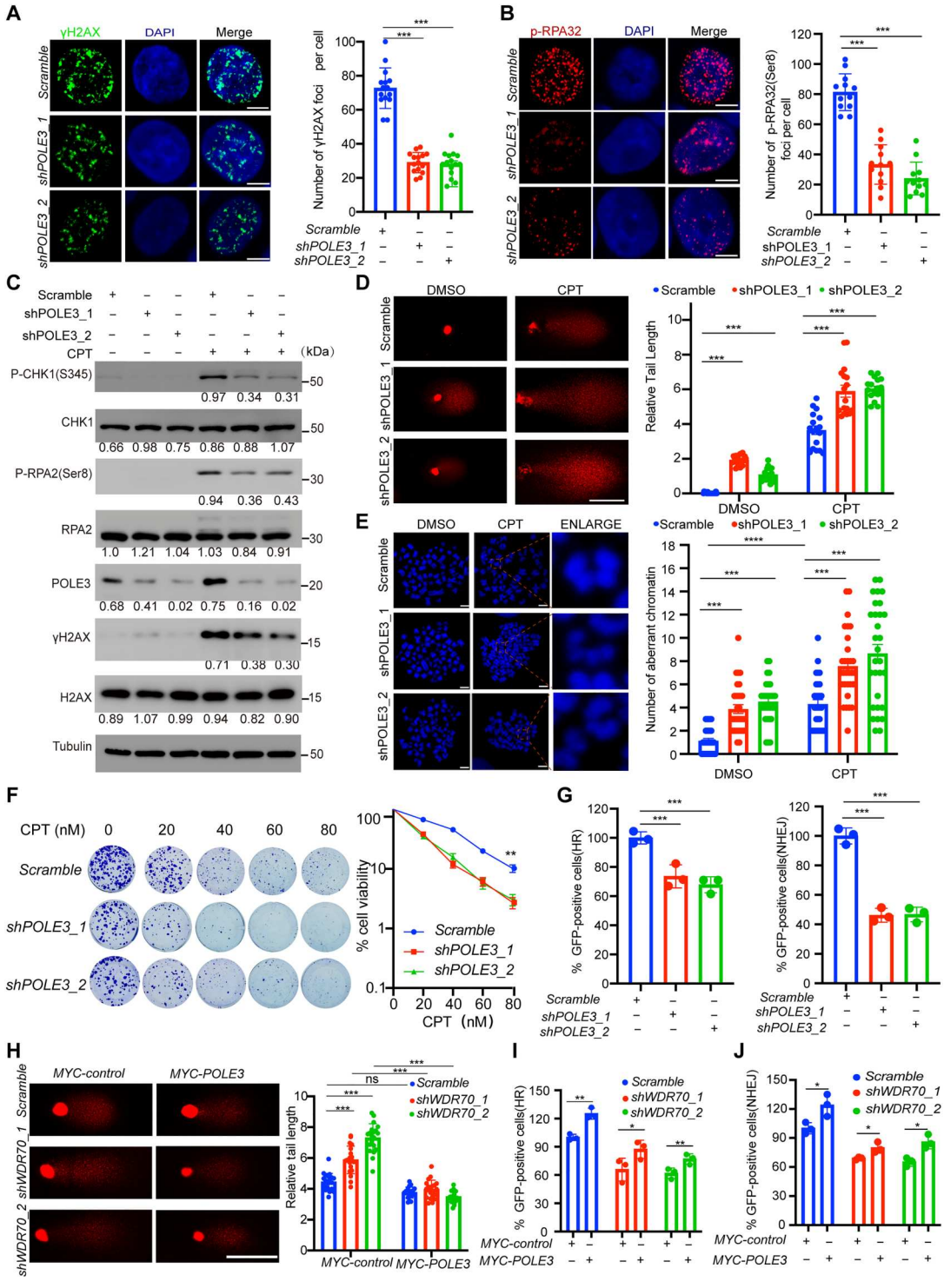

Fig. 5. Effect of POLE3 depletion on DDR. (**A** and **B**) Representative images of γH2AX foci (A), phosphorylated RPA2 (p-RPA32) foci (B), and DAPI-stained nuclei in control or shPOLE3 HCT116 cells treated with CPT for 4 hours (left). Scale bars, 5 μm. Quantification of γH2AX foci per cell and p-RPA32 foci per cell (right). The number from three independent experiments is shown. (**C**) Western blotting analysis showing the indicated proteins in HCT116 cells under the same conditions as (A). (**D**) Direct observation of DNA damage in HCT116 cells treated with CPT for 12 hours. Representative images are shown. Scale bar, 50 μm. Quantitation of the comet data (right). (**E**) Representative images of aberrant chromosomes. HCT116 cells with or without POLE3 knockdown was treated with CPT followed by karyotype assay. Scale bars, 5 μm. Quantitation of aberrant chromosomes per cells (right). Total 30 cells were counted in each group. (**F**) Representative images of colony formation (left) and survival curves (right). Cell viability based on clonogenic growth of HCT116 cells in the presence of CPT for 24 hours. (**G**) The efficiency assay of HR (left) and NHEJ (right) for chromosomal DSB induced by endonuclease I-Sce I. HR and NHEJ efficiency were determined in POLE3-deficient cells by FACS-based fluorescence readout. (**H**) Direct observation of DNA damage in WDR70-deficient cells with ectopic expression of MYC-POLE3 after CPT treatment for 48 hours (left). Scale bar, 50 μm. Quantitation of the comet data (right). HR efficiency (**I**) and NHEJ efficiency (**J**) in WDR70-deficient cells with or without ectopic expression of MYC-POLE3. The results are shown as mean ± SD (n = 3). Error bars represent SD. *P < 0.05, **P < 0.01, and ***P < 0.001.

CHRAC1^{D121Y} identified in patient with CRC attenuates the interaction with POLE3

Our data have shown that WDR70 is required for genome integrity. Another study also supports this notion by showing that WDR70 loss elicits hallmarks of gnomic instability by reducing the expression of DDR factors, including BRCA1, BRCA2, RAD51, and other HDR factors (*20*). Thus, we speculate that the aberrant expression of WDR70 and POLE3 is possibly involved in tumorigenesis or tumor development. By analyzing The Cancer Genome Atlas (TCGA) data, we observed the notable positive correlation between POLE3 and WDR70 expression in cancer (Fig. 8A). Consistent with the results of TCGA, the elevated expression of POLE3 and WDR70 was also observed in CRC tissues (Fig. 8B). Intriguingly, by whole-exome sequencing 24 paired-CRC tissues, we characterized

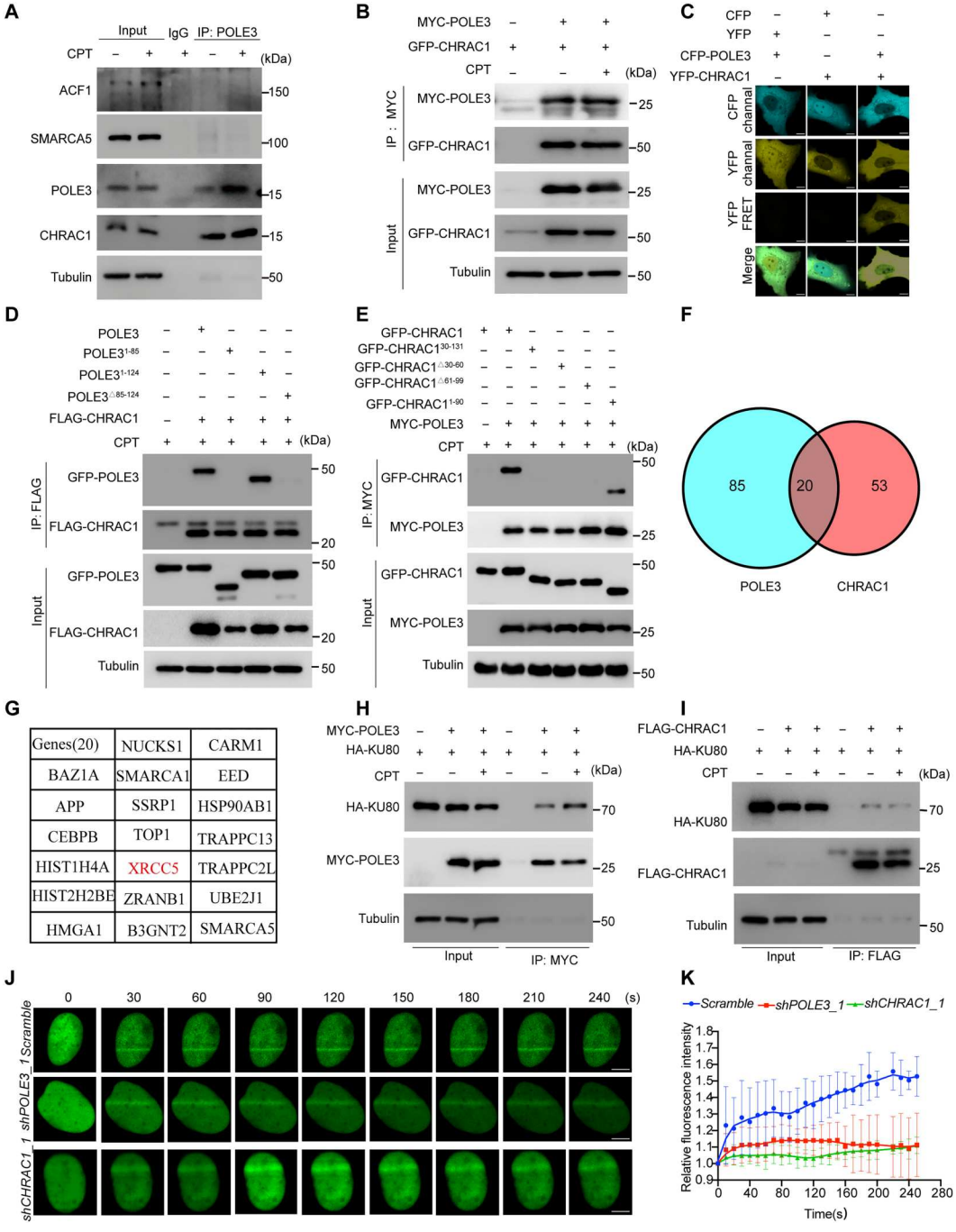

Fig. 6. POLE3 interacts with CHRAC1 to recruit KU80 to DNA damage sites. (**A** and **B**) Coimmunoprecipitation of endogenous POLE3 (A) or ectopically expressed POLE3 (B) with CHRAC1. The lysates of HCT116 cells (A) and HEK293T cells cotransfected with *MYC-POLE3* and *GFP-CHRAC1* (B) were subjected to immunoprecipitation using anti-POLE3 antibody or anti-MYC magnetic beads, respectively. After immunoprecipitation, immunoblots were performed with the indicated antibodies. (**C**) Visualization of POLE3-CHRAC1 interaction using FRET assay. Representative images of FRET acceptor photobleaching assay of HEK293T cells cotransfected with *POLE3-CFP* and *CHRAC1-YFP*. Scale bars, 20 μm. (**D**) Coimmunoprecipitation of wild-type and truncated POLE3 with CHRAC1. Whole-cell extracts of HEK293T cells cotransfected with *GFP-POLE3* and *FLAG-CHRAC1* were subjected to immunoprecipitation using M2 magnetic beads. Captured proteins were detected by Western blotting using specific antibodies as indicated. (**E**) Coimmunoprecipitation of wild-type or truncated CHRAC1 with POLE3. Whole-cell extracts of HEK293T cells cotransfected with *GFP-CHRAC1* and *MYC-POLE3* were subjected to immunoprecipitation using anti-MYC antibody. Captured proteins were detected by Western blotting using specific antibodies as indicated. (**F**) Venn diagram displays the proteins associated with POLE3 and CHRAC1. (**G**) Proteins interacting with both POLE3 and CHRAC1. (**H** and **I**) Coimmunoprecipitation of POLE3 (H) and CHRAC1 (I) with KU80. Whole-cell extracts of HEK293T cells cotransfected with *MYC-POLE3* or *FLAG-CHRAC1* and *HA-KU80* were subjected to immunoprecipitation using anti-MYC or M2 magnetic beads. Captured proteins were detected by Western blotting using specific antibodies as indicated. (**J**) Representative images of KU80 recruitment at DNA damage sites generated by laser microirradiation in control, shPOLE3, or shCHRAC1 U2OS cells treated with Hoechst (1 μg/ml) for 15 min. Scale bars, 5 μm. (**K**) Quantification of EGFP-KU80 relative fluorescence intensity at laser-microirradiated regions. Each measurement is representative of at least 10 cells and the experiment was independently repeated at least three times.

the mutation spectrum of well-known genes involved in CRC such as *APC*, *KRAS*, *NRAS*, *TP53*, and *PIK3CA* (Fig. 8C). Intriguingly, D121Y mutation in CHRAC1 was identified and further confirmed this mutation in patient with CRC using PCR followed by sequencing (Fig. 8, C and D). In addition, loss of CHRAC1 showed the starched comet tails in cells, which was abolished by ectopically expressing wild-type but not by D121Y mutant of CHRAC1 (Fig. 8, E and F). Consistent with the result of comet assay, the D121Y mutant failed to rescue the cell viability in response to CPT (fig. S5), confirming the significance of CHRAC1 in DDR. The direct interaction between POLE3 and CHRAC1 prompted us to ask whether the D121Y mutation affect the interaction. In contrast to wild-type CHRAC1, D121Y mutation attenuated the association with POLE3 detected by coimmunoprecipitation (Fig. 8G). Together,

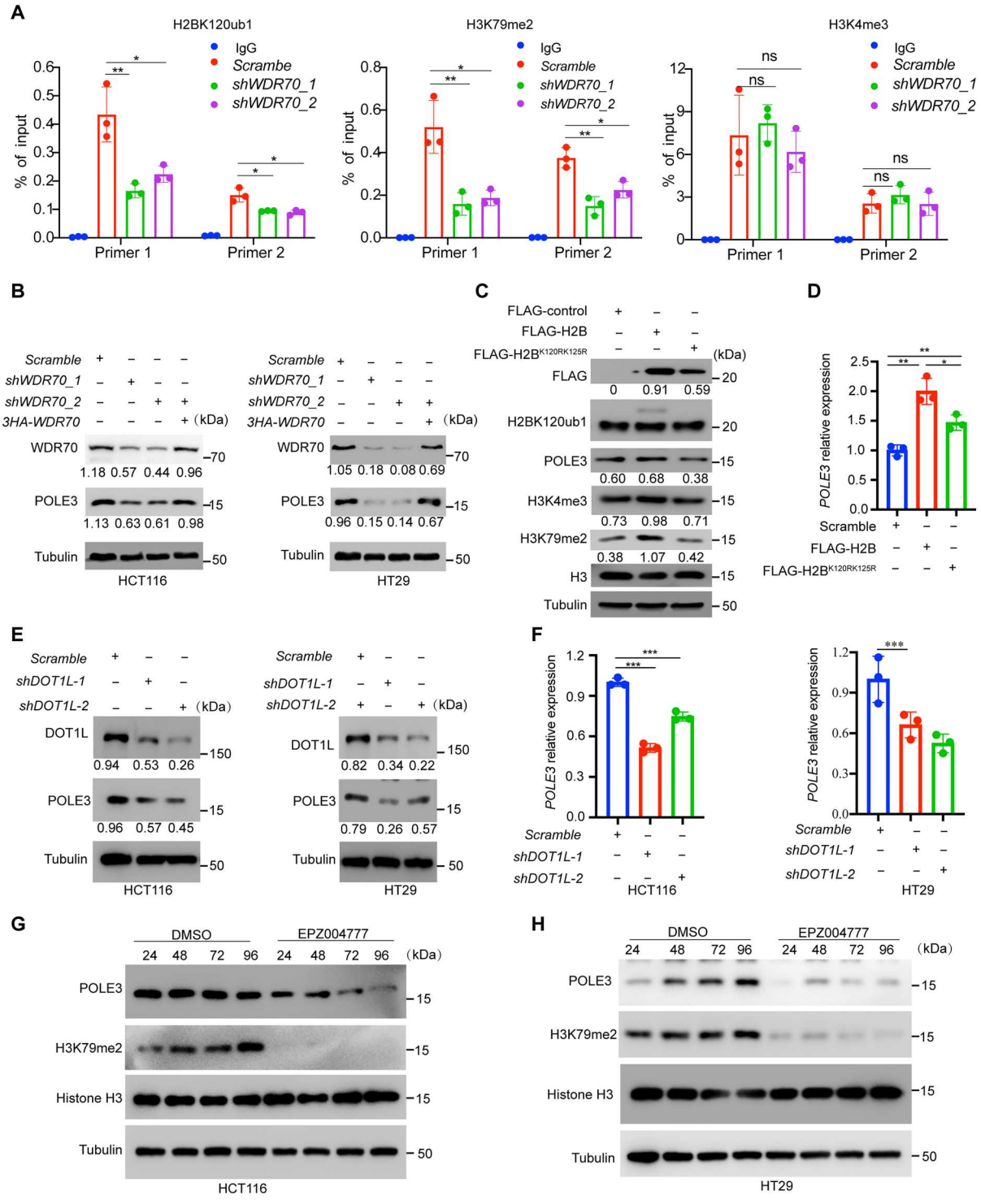

Fig. 7. The influence of WDR70, H2BK120UB1, and H3K79me2 on POLE3 expression in cells. (**A**) The enrichment of H2BK120ub1, H3K79me2, and H3K4me3 at *POLE3* loci detected by ChIP. Lysates from WDR70 knockdown cells were subjected to ChIP assay using specific antibodies against H2BK120ub1, H3K4me3, and H3K79me2. Each ChIP experiment was performed independently at least three times, with results from on representative experiment shown. **P* < 0.05, ***P* < 0.01, and ****P* < 0.001. (**B**) Representative Western blot analysis in HCT116 and HT29 cells with WDR70 knockdown. Quantification of indicated protein band intensity plotted relative to tubulin. (**C** and **D**) Representative Western blot analysis (C) and quantitative RT-PCR analysis for POLE3 expression (D) in cells with the ectopic expression of wild-type and H2BK120R K125R and quantification of indicated protein band intensity plotted relative to tubulin. (**E** and **F**) Representative Western blot analysis (E) and quantitative RT-PCR analysis (F) for POLE3 expression in HCT116 and HT29 cells with DOT1L knockdown. Number represents the quantification of indicated protein band intensity plotted relative to tubulin. qRT-PCR experiment was performed independently at least three times, with results from on representative experiment shown. **P* < 0.05, ***P* < 0.01, and ****P* < 0.001. (**G** and **H**) Representative Western blot analysis in HCT116 (G) and HT29 (H) cells treated with DOT1L inhibitor EPZ004777.

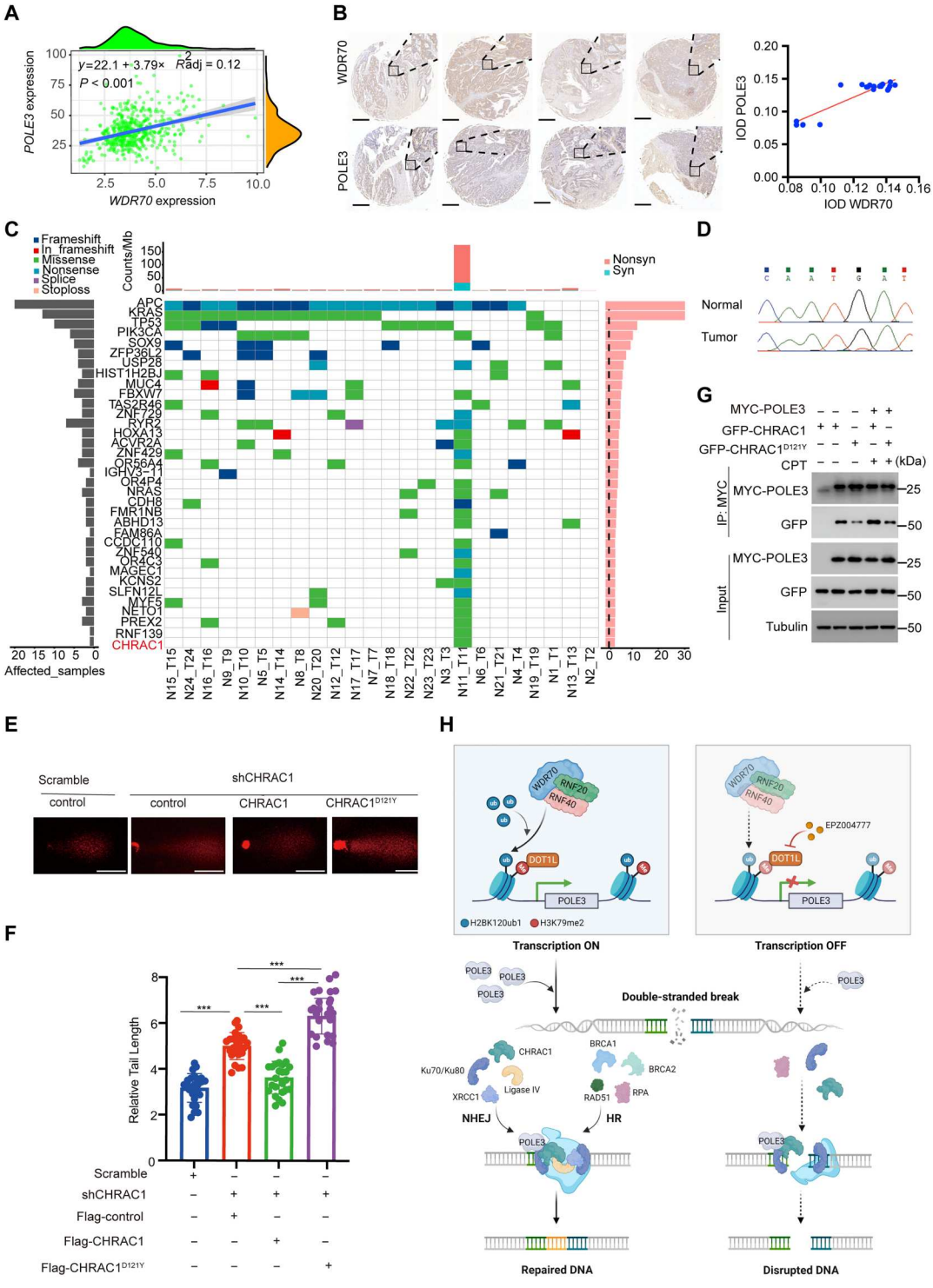

Fig. 8. CHRAC1^{D121Y} mutation identified in patients with CRC weakens the interaction between POLE3 and CHRAC1. (**A**) Positive correlation between WDR70 and POLE3 in CRC patients. (**B**) Representative images of IHC staining for WDR70 and POLE3 in patients with CRC. (**C**) Spectrum and frequency of susceptibility gene mutation in patients with CRC analyzed by whole-exome sequencing. Twenty-four paired-CRC tissues were subjected to whole-exome sequencing. Each row represents a gene, and each column represents a patient. Different mutation types are indicated by different colors. The bar chart on the left shows the given gene's mutation observed in the sample. (**D**) Identification and validation of CHRAC1^{D121Y} mutation in CRC by sequencing. (**E**) Direct observation of DNA damage by using the comet assay in CHRAC1-deficient cells with ectopic expression of wild-type and D121Y mutant of CHRAC1 after CPT treatment for 12 hours. Representative images are shown. Scale bars, 50 μm. (**F**) Quantitation of the comet data. Error bars represent SEM. *P < 0.05, **P < 0.01, and ***P < 0.001. (**G**) Coimmunoprecipitation of CHRAC1 D121Y mutant with POLE3. Whole-cell extracts of HEK293T cells co-transfected with *MYC-POLE3* and *GFP-CHRAC1* were subjected to immunoprecipitation using anti-MYC magnetic beads. Captured proteins were detected by Western blotting using specific antibodies as indicated. (**H**) Model for WDR70-RNA20/40 function at DSBs. After DSB formation, WDR70 functions with RNF20/40 synergistically to catalyze histone H2BK120ub1, which in turn promotes H3K79me2 at *POLE3* loci and eventually facilitates *POLE3* transcription. POLE3 in complex with CHRAC1 enhances the expression of HDR proteins and the recruitment of KU80 at DNA damage sites, allowing DNA repair via NHEJ and HR pathway.

these results suggest that the aberrant POLE3-CHRAC1 interaction is probably implicated in CRC development through hindering DDR.

DISCUSSION

The monoubiquitylation of H2B mediated by RNF20/40 has an established role in the regulation of transcription and in DDR (*9*, *12*, *13*, *15*). WDR70 functions as a subunit of CRL4 complex in HDR by regulating the transcription of *BRCA1*, *BRCA2*, *RAD51*, and substantial additional transcriptomic changes (*20*). In addition, CRL4^{WDR70} could promote the monoubiquitylation of H2B to

affect DNA resection and thus HDR (*21*). Despite all these, our current understanding of the factors that regulate H2BK120ub1 in DDR needs to be further polished. By using the affinity purification mass spectrometry, we identified a broad profile of proteins associated with WDR70, including H2B monoubiquitylation E3 ligase RNF20/40, and also revealed that WD40 repeats in WDR70 are required for the interaction with RNF20/40. H2BK120ub1 level was reduced after WDR70 knockdown, and the reduction was not recovered by overexpression of WDR70 lacking entire WD40 repeats or by overexpression of RNF20/40, implying that WD40 repeats in WDR70 contributes substantially to the interaction with RNF20/40 and therefore de novo H2BK120ub1. Although the interaction between WDR70 and RNF20/40 is validated in vivo, it is worth to further investigate the interaction by protein crystallization to identify structural basis to clarify whether the interaction is direct.

What notable phenotypes could be led by WDR70 loss in cells? It is expected that one obvious phenomenon is genomic instability (*20*, *21*), as WDR70 deficiency leads to the reduction of H2BK120ub1 and DDR-related proteins, which eventually crashes the DNA repair pathway like HR and NHEJ. We showed that WDR70 loss has a pronounced effect on not only HDR proteins but also POLE3, a histone-fold protein that interacts with POLE4 to bind DNA in a sequence-independent manner and to function as a histone H3-H4 chaperone (*36*). WDR70 loss had a predominant effect on cellular mRNA levels, including the reduction of *POLE3* transcripts, which corresponded to the loss at the protein level. It has been reported that POLE3 promotes checkpoint activation, and loss of POLE3 enhances cells′ sensitivity to ATR inhibitor, PARP inhibitor, and CPT (*33*–*35*). Therefore, the regulation on POLE3 by WDR70 hints at a connection between H2BK120ub1 and POLE3 transcription in DDR. The enrichment of H2BK120ub1 and H3K79me2 at POLE3 loci and the failure of elevation in POLE3 expression by ectopic H2B2KR that the incorporation into the chromatin of mutant H2B strictly block H2B monoubiquitylation and consequently H2BK120ub1-driven processes in cells point out the significance of WDR70 and H2BK120ub1 in *POLE3* transcription.

Although our works established WDR70-H2BK120ub1 axis as a key factor in regulation of POLE3 expression, how this network is coordinated in the context of DDR and whether POLE3 cooperates with other proteins at DNA damage sites remains to be determined. POLE3, together with ACF1, SMARCA5, and CHRAC1, could form CHRAC at DNA damage sites (*38*, *42*). Thus, it would be tempting to speculate that CHRAC complex containing POLE3 might promote DNA repair. Our data support this possibility since coimmunoprecipitation assay showed that POLE3 directly interacts with CHRAC1 in cells treated with CPT. We observed the interaction between POLE3 and KU80 and the enhanced interaction after induced DNA break by CPT. A noteworthy finding was that a preference for KU80 recruitment at DNA damage sites in vivo, suggesting that POLE3-CHRAC1 complex plays a critical role in recruiting or constraining KU70/80 complex at DNA damage sites to fulfill the repair function. RNF20 depletion also causes the defect of YFP-KU80 recruitment at laser-induced damage sites (*12*), supporting our discovery that H2BK120ub1 drives *POLE3* transcription, which in turn enhances the KU80 recruitment. In future studies, it will be important to understand whether ACF1, which has been previously shown to function as a KU70-binding protein (*38*), is coordinated with POLE3 in recruiting or constraining KU70/80 complex at DNA damage sites.

Gene expression is tightly regulated by dynamic chromatin states controlled by multiple families of chromatin regulators including the modifiers of DNA methylation, histone methylation and ubiquitylation, and chromatin remodeling complexes. The mutation of chromatin regulators is frequently observed in human cancer and thus these regulators are attractive drug targets (*43*–*48*). Our results also highlight the importance of chromatin regulators in cancer by showing D121Y mutation of CHRAC1 in CRCs, which has a great challenge in POLE3 interaction and the recruitment of KU70/80 complex in DDR. Genomic instability and accumulation of unrepaired DSBs are a common problem in many malignancies, as cancer cell is bombarded with numerous DNA-damaging events (*49*, *50*). Therefore, our work implies that POLE3 or aberrant CHRAC1 may be exploitable as cancer cell–specific therapeutic targets.

Collectively, our data suggest a model that WDR70-RNF20/40-H2Bub1 pathway is required for the DSB repair process. In particular, our studies reveal a link between WDR70-RNF20/40-H2Bub1 and POLE3, and this functional link leads to the increase in *POLE3* transcription via chromatin relaxation at *POLE3* loci. Increased POLE3 could enhance the interaction with CHRAC1; elevate the level of γH2AX, p-RPA2, and phosphorylated CHK1; and recruit or constrain KU70/80 complex at DNA damage sites to ensure DNA repair by HR and NHEJ pathway (Fig. 8H).

MATERIALS AND METHODS

Cell culture

HEK293T, HCT116, and HT29 were purchased from the cell bank of the Chinese Academy of Science (Shanghai, China). All cell lines were confirmed by short tandem repeat (STR) analysis before use. Cells were cultured in Dulbecco′s modified Eagle′s medium (ExCell) with 10% fetal bovine serum, 100 U of streptomycin, and penicillin (100 μg/ml) at 37°C in atmosphere of 5% CO_2.

Western blot

Total proteins were extracted from cells using SDS-containing lysis buffer plus 1× protease inhibitor cocktail. The protein lysates were separated on 6 to 15% SDS–polyacrylamide gel electrophoresis (PAGE) gel according to the molecular weight of target proteins and subsequently transferred onto polyvinylidene difluoride membranes with a 0.2-μm pore size. Following transfer, membranes were blocked in tris-buffered saline (TBS) buffer with 5% milk and 0.1% Tween 20 for 1 hour at room temperature and then incubated with indicated primary antibody overnight at 4°C. After being washed for three times with TBS buffer containing 0.1% Tween 20, the membrane was incubated with secondary antibody for 1 hour at room temperature. The immunoblotting band was detected by an enhanced chemiluminescence detection kit, and the quantifications of Western blot bands were conducted by ImageJ software [National Institutes of Health (NIH)]. Antibodies used in this study were listed in table S1.

RNA extraction, quantitative RT-PCR, and RNA sequencing

Total RNA was extracted from cells with TRIzol (Invitrogen, USA) according to the manufacturer′s instructions and stored in diethyl pyrocarbonate–treated water. The complementary DNA (cDNA)

was reverse transcribed using PrimeScript II first Strand cDNA Synthesis Kit (Takara, 6210A). Quantitative real-time PCR (qRT-PCR) was performed using NovoStartSYBR qPCR SuperMix plus (Novoprotein, E096). The fold change of target gene was calculated by normalization with housekeeping gene *ACTIN* using the ddCt methods. For RNA sequencing, briefly, the total RNA was extracted from cells for preparing library, and RNA sequencing was conducted on a HiSeqTM 200 platform (Illumina, USA). Primers and oligos used in this study were listed in tables S1 and S2.

Immunoprecipitation assay

The cells were washed with phosphate-buffered saline (PBS) buffer and collected by centrifugation with enzyme disaggregation. The cell pellet was resuspended with immunoprecipitation lysis buffer (20 mM tris, 137 mM NaCl, 5% glycerol, 1% NP-40, and 2 mM MEDTA, pH 7.5) plus protease inhibitors for 30 min at 4°C. The resulted supernatant was subjected to immunoprecipitation using specific antibodies against target genes or anti-tag antibody coated magnetic beads for 2 hours or overnight at 4°C with rotation. The beads were washed three times for 5 min with washing buffer. The protein bound to beads was eluted with loading buffer and analyzed by Western blotting.

Cell colony formation assay

Cells were counted and subsequently were seeded in 48-well plates at 500 cells per well and incubated at 37°C in humidified incubator. Upon adherent to plate, cells were treated with indicated drugs for 24 hours. Subsequently, cells were supplemented with fresh medium three times a week. Last, cells were fixed by 4% paraformaldehyde (PFA) for 30 min and stained with 0.1% crystal violet for 20 min at room temperature after 2 weeks. The total number of cell colonies was counted at the end of experiments.

Comet assay

Comet assay was performed following the protocol published previously (*51*). Briefly, after washed for three times with PBS buffer, cells were mixed in low-melting agarose. After lysis, samples were pipetted onto the slides, which were previously coated with low-melting agarose. Then slides were submerged in alkaline lysis buffer at 4°C overnight in the dark. Slides were subjected to electrophoresis for 25 min at a voltage of 0.6 V/cm followed by staining with EB for 10 min. Images of randomly selected cells per sample were captured by using an LSM880 Zeiss laser confocal microscope. The relative DNA tail length was measured using ImageJ software (NIH). The relative length and intensity of DNA tails relative to heads is proportional to the amount of DNA damage in individual nuclei.

Micronuclei quantitation

Cells were fixed by using 4% PFA and subsequently treated with 0.3% Triton X-100 for 15 min. The slides were stained with Hoechst 33342 for 15 min and washed three times with PBS buffer. The image was captured by using a LSM880 Zeiss laser confocal microscope. Greater than 200 cells were imaged. The data shown are the mean ± SE.

Karyotype assay

Cells were treated with colchicine (1 μg/ml) for 2 hours before harvest and were resuspended with 75 mM KCl for 25 min in a water bath (37°C). The cell suspensions were centrifugated at 1000 rpm for 10 min. The resulted pellets were fixed with 7 ml of fresh Carnoy (methanol:acetic acid = 3:1) for 10 min, and the suspension was centrifugated again. Pellets were resuspended with a few drops of Carnoy. The suspensions were dropped onto a precleaned slide. After being dried at room temperature, the slides were stained with 4′,6-diamidino-2-phenylindole (DAPI) and metaphase chromosomes were captured by using an LSM880 Zeiss laser confocal microscope.

Immunofluorescence staining and whole-exome sequencing

Cells were seeded into 24-well plates with glass coverslips at 5000 per well for 2 days. After being washed with PBS buffer, cells were fixed with 4% PFA, and permeabilized with 0.3% Triton X-100 in PBS buffer for 15 min followed by incubation with 5% fatal bovine serum for 30 min at room temperature. Cells were indicated with primary antibody at 4°C overnight. After washing with PBS buffer, cells were incubated with indicated secondary antibody for 1 hour at room temperature. Last, images were captured using LSM880 laser confocal microscope.

For whole-exome sequencing of human colorectal tumors, paired adjacent normal mucosa, the samples were obtained from the West China Hospital (Chengdu, China). All patients signed informed written consent with the approval of the Biological and Medical Ethics Committee of West China Hospital. Whole-exosome sequencing was conducted on a Hiseq X-Ten PE150 (Illumina, USA) by OE Biotech Co, Ltd (Shanghai, China).

Laser microirradiation analysis

The LSM880 ZEISS laser confocal microscope was applied to irradiation by a 405-nm laser. Cells were incubated with Opti-MEM plus 10% fetal bovine serum without phenol and administrated with Hoechst (10 μg/ml) to increase sensitivity for laser before laser microirradiation. Cells were scanned for 30 times with 405-nm laser at 70%, one iteration, zoom of 3, and pixel dwell time of 12.61 μs. After treatment with laser irradiation, time-lapse images were taken with an LSM880 ZEISS laser confocal microscope.

Chromatin immunoprecipitation

ChIP assay was performed according to the protocol published previously (*52*, *53*). Briefly, cells were cross-linked with 1% PFA (Sigma-Aldrich) followed by quenching the reaction with 125 mM glycine. After being washed twice with PBS buffer, cell pellets were transferred to a microfuge tube. Cells were administrated with lysis buffer plus protease inhibitors and sonicated to about 500-bp fragments. The supernatant was collected by centrifugation at 10,800 rpm for 15 min and diluted 10-fold with ChIP dilution buffer plus protease inhibitors. The chromatin supernatant was incubated with primary antibody at 4°C overnight. The protein G agarose beads were washed with ChIP dilution buffer for several times and incubated with the resulted supernatant for 3 hours. The beads were sequentially washed for 5 min at 4°C with low-salt buffer, high-salt buffer, LiCl buffer, and Tris-EDTA (TE) buffer. DNA fragments were enriched with 10% chelex (Bio-Rad). Immunoprecipitated DNA was analyzed by qRT-PCR with specific primers for target genes.

HR repair assay

Site-specific recombination after DSB induction by I-Sce I was determined as described previously (*54*). Briefly, DR-U2OS cells were transfected with I-Sce I–expressing vector or an empty vector for 72 hours. The cells were harvested with enzyme disaggregation and then were resuspended in PBS buffer supplemented with 10% fetal bovine serum. FACSort flow cytometer was used to sort the GFP-positive cells at 10,000 events per sample. The results were analyzed by FlowJo software.

NHEJ assay

NHEJ assay was conducted according to the protocol published previously (*54*). The EJ5-GFP cells were transfected with an I-Sce I–expressing vector or an empty vector for 72 hours. The cells were harvested with enzyme disaggregation and were resuspended in PBS buffer supplemented with 10% fetal bovine serum. FACSort flow cytometer was used to sort the GFP-positive cells at 10,000 events per sample. The results were analyzed by FlowJo software.

Immunohistochemistry staining

The clinical colorectal tissue microarray was purchased from Outdo Biotech Company (Shanghai, China). All samples were embedded in paraffin, deparaffinized, and rehydrated in advance. For immunohistochemistry staining, the tissue was boiled in sodium citrate buffer for 90 s to retrieval antigen followed by treatment with 3% H_2O_2 for 10 min and blocking with 1% bovine serum albumin solution for 15 min. The specific antibodies against POLE3 (ABclonal, A6469) and WDR70 (HUABIO) were incubated at 4°C overnight in a humidified chamber. After 30-min incubation with the secondary antibody at room temperature, the slides were stained with hematoxylin and 3,3′diaminobenzidine.

Detection of protein ubiquitination in vivo

HEK293T cells were cotransfected with the plasmid of FLAG-tagged ubiquitin and the indicated MYC-tagged gene for 48 hours. Cell lysates were prepared and subjected to immunoprecipitation using anti-FLAG or anti-MYC antibody–coupled magnetic beads. After extensively washing out unbound proteins, captured proteins were detected by Western blot using specific antibodies.

Gene expression analysis

The gene expression data were retrieved from TCGA (https://portal.gdc.cancer.gov/) database, and the correlation between *WDR70* mRNA expression and *POLE3* mRNA expression was analyzed in colorectal (n = 530) and normal tissues (n = 42) by R software with ggplot2 package.

Ethics approval and consent to participate

Use of human tissues was reviewed and approved by the ethics committee of West China Hospital of Sichuan University.

Statistical analysis

All quantitative data were analyzed using GraphPad (v9.0) software, and the values were shown as mean ± SD. Student's t test was applied to determine the comparison of difference where appropriate. $P < 0.05$ was considered as statistical significance.

Supplementary Materials

This PDF file includes:

Figs. S1 to S5
Tables S1 to S3

REFERENCES AND NOTES

1. D. Hanahan, R. A. Weinberg, Hallmarks of cancer: The next generation. *Cell* **144**, 646–674 (2011).
2. D. Hanahan, Hallmarks of cancer: New dimensions. *Cancer Discov.* **12**, 31–46 (2022).
3. S. C. West, Molecular views of recombination proteins and their control. *Nat. Rev. Mol. Cell Biol.* **4**, 435–445 (2003).
4. M. R. Lieber, The mechanism of double-strand DNA break repair by the nonhomologous DNA end-joining pathway. *Annu. Rev. Biochem.* **79**, 181–211 (2010).
5. R. Oz, S. M. Howard, R. Sharma, H. Tornkvist, I. Ceppi, S. Kk, E. Kristiansson, P. Cejka, F. Westerlund, Phosphorylated CtIP bridges DNA to promote annealing of broken ends. *Proc. Natl. Acad. Sci. U.S.A.* **117**, 21403–21412 (2020).
6. S.-Y. Jeong, G. Hariharasudhan, M.-J. Kim, J.-Y. Lim, S. M. Jung, E.-J. Choi, I.-Y. Chang, Y. Kee, H. J. You, J.-H. Lee, SIAH2 regulates DNA end resection and replication fork recovery by promoting CtIP ubiquitination. *Nucleic Acids Res.* **50**, 10469–10486 (2022).
7. X. Chen, X. Xu, Y. Chen, J. C. Cheung, H. Wang, J. Jiang, N. de Val, T. Fox, M. Gellert, W. Yang, Structure of an activated DNA-PK and its implications for NHEJ. *Mol. Cell* **81**, 801–810.e3 (2021).
8. Z. W. Sun, C. D. Allis, Ubiquitination of histone H2B regulates H3 methylation and gene silencing in yeast. *Nature* **418**, 104–108 (2002).
9. R. K. McGinty, J. Kim, C. Chatterjee, R. G. Roeder, T. W. Muir, Chemically ubiquitylated histone H2B stimulates hDot1L-mediated intranucleosomal methylation. *Nature* **453**, 812–816 (2008).
10. R. Pavri, B. Zhu, G. Li, P. Trojer, S. Mandal, A. Shilatifard, D. Reinberg, Histone H2B monoubiquitination functions cooperatively with FACT to regulate elongation by RNA polymerase II. *Cell* **125**, 703–717 (2006).
11. B. Fierz, C. Chatterjee, R. K. McGinty, M. Bar-Dagan, D. P. Raleigh, T. W. Muir, Histone H2B ubiquitylation disrupts local and higher-order chromatin compaction. *Nat. Chem. Biol.* **7**, 113–119 (2011).
12. L. Moyal, Y. Lerenthal, M. Gana-Weisz, G. Mass, S. So, S. Y. Wang, B. Eppink, Y. M. Chung, G. Shalev, E. Shema, D. Shkedy, N. I. Smorodinsky, N. van Vliet, B. Kuster, M. Mann, A. Ciechanover, J. Dahm-Daphi, R. Kanaar, M. C. Hu, D. J. Chen, M. Oren, Y. Shiloh, Requirement of ATM-dependent monoubiquitylation of histone H2B for timely repair of DNA double-strand breaks. *Mol. Cell* **41**, 529–542 (2011).
13. P. Schwertman, S. Bekker-Jensen, N. Mailand, Regulation of DNA double-strand break repair by ubiquitin and ubiquitin-like modifiers. *Nat. Rev. Mol. Cell Biol.* **17**, 379–394 (2016).
14. N. Minsky, M. Oren, The RING domain of Mdm2 mediates histone ubiquitylation and transcriptional repression. *Mol. Cell* **16**, 631–639 (2004).
15. J. Kim, M. Guermah, R. K. McGinty, J. S. Lee, Z. Tang, T. A. Milne, A. Shilatifard, T. W. Muir, R. G. Roeder, RAD6-mediated transcription-coupled H2B ubiquitylation directly stimulates H3K4 methylation in human cells. *Cell* **137**, 459–471 (2009).
16. G. Fuchs, M. Oren, Writing and reading H2B monoubiquitylation. *Biochim. Biophys. Acta* **1839**, 694–701 (2014).
17. A. Wood, N. J. Krogan, J. Dover, J. Schneider, J. Heidt, M. A. Boateng, K. Dean, A. Golshani, Y. Zhang, J. F. Greenblatt, M. Johnston, A. Shilatifard, Bre1, an E3 ubiquitin ligase required for recruitment and substrate selection of Rad6 at a promoter. *Mol. Cell* **11**, 267–274 (2003).
18. J. Dover, J. Schneider, M. A. Tawiah-Boateng, A. Wood, K. Dean, M. Johnston, A. Shilatifard, Methylation of histone H3 by COMPASS requires ubiquitination of histone H2B by Rad6. *J. Biol. Chem.* **277**, 28368–28371 (2002).
19. J. S. Lee, A. Shukla, J. Schneider, S. K. Swanson, M. P. Washburn, L. Florens, S. R. Bhaumik, A. Shilatifard, Histone crosstalk between H2B monoubiquitination and H3 methylation mediated by COMPASS. *Cell* **131**, 1084–1096 (2007).
20. Z. Mirman, K. Sharma, T. S. Carroll, T. de Lange, Expression of BRCA1, BRCA2, RAD51, and other DSB repair factors is regulated by CRL4WDR70. *DNA Repair* **113**, 103320 (2022).
21. M. Zeng, L. Ren, K. Mizuno, K. Nestoras, H. Wang, Z. Tang, L. Guo, D. Kong, Q. Hu, Q. He, L. Du, A. M. Carr, C. Liu, CRL4(Wdr70) regulates H2B monoubiquitination and facilitates Exo1-dependent resection. *Nat. Commun.* **7**, 11364 (2016).
22. R. A. Poot, G. Dellaire, B. B. Hulsmann, M. A. Grimaldi, D. F. Corona, P. B. Becker, W. A. Bickmore, P. D. Varga-Weisz, HuCHRAC, a human ISWI chromatin remodelling complex contains hACF1 and two novel histone-fold proteins. *EMBO J.* **19**, 3377–3387 (2000).

23. G. LeRoy, A. Loyola, W. S. Lane, D. Reinberg, Purification and characterization of a human factor that assembles and remodels chromatin. *J. Biol. Chem.* **275**, 14787–14790 (2000).
24. F. Zhang, X. Yu, WAC, a functional partner of RNF20/40, regulates histone H2B ubiquitination and gene transcription. *Mol. Cell* **41**, 384–397 (2011).
25. N. Pashkova, L. Gakhar, S. C. Winistorfer, L. Yu, S. Ramaswamy, R. C. Piper, WD40 repeat propellers define a ubiquitin-binding domain that regulates turnover of F box proteins. *Mol. Cell* **40**, 433–443 (2010).
26. C. C. So, S. Ramachandran, A. Martin, E3 ubiquitin ligases RNF20 and RNF40 are required for double-stranded break (DSB) repair: Evidence for monoubiquitination of histone H2B lysine 120 as a novel axis of DSB signaling and repair. *Mol. Cell. Biol.* **39**, e00488-18 (2019).
27. T. Prenzel, Y. Begus-Nahrmann, F. Kramer, M. Hennion, C. Hsu, T. Gorsler, C. Hintermair, D. Eick, E. Kremmer, M. Simons, T. Beissbarth, S. A. Johnsen, Estrogen-dependent gene transcription in human breast cancer cells relies upon proteasome-dependent monoubiquitination of histone H2B. *Cancer Res.* **71**, 5739–5753 (2011).
28. Z. Wang, L. Zhu, T. Guo, Y. Wang, J. Yang, Decreased H2B monoubiquitination and overexpression of ubiquitin-specific protease enzyme 22 in malignant colon carcinoma. *Hum. Pathol.* **46**, 1006–1014 (2015).
29. K. Nakamura, A. Kato, J. Kobayashi, H. Yanagihara, S. Sakamoto, D. V. Oliveira, M. Shimada, H. Tauchi, H. Suzuki, S. Tashiro, L. Zou, K. Komatsu, Regulation of homologous recombination by RNF20-dependent H2B ubiquitination. *Mol. Cell* **41**, 515–528 (2011).
30. G. Liu, J. Yan, X. Wang, J. Chen, X. Wang, Y. Dong, S. Zhang, X. Gan, J. Huang, X. Chen, RPA-mediated recruitment of Bre1 couples histone H2B ubiquitination to DNA replication and repair. *Proc. Natl. Acad. Sci. U.S.A.* **118**, e2017497118 (2021).
31. E. Shema, J. Kim, R. G. Roeder, M. Oren, RNF20 inhibits TFIIS-facilitated transcriptional elongation to suppress pro-oncogenic gene expression. *Mol. Cell* **42**, 477–488 (2011).
32. B. Fierz, S. Kilic, A. R. Hieb, K. Luger, T. W. Muir, Stability of nucleosomes containing homogenously ubiquitylated H2A and H2B prepared using semisynthesis. *J. Am. Chem. Soc.* **134**, 19548–19551 (2012).
33. N. Hustedt, A. Alvarez-Quilon, A. McEwan, J. Y. Yuan, T. Cho, L. Koob, T. Hart, D. Durocher, A consensus set of genetic vulnerabilities to ATR inhibition. *Open Biol.* **9**, 190156 (2019).
34. D. Su, X. Feng, M. Colic, Y. Wang, C. Zhang, C. Wang, M. Tang, T. Hart, J. Chen, CRISPR/CAS9-based DNA damage response screens reveal gene-drug interactions. *DNA Repair (Amst)* **87**, 102803 (2020).
35. E. Casari, E. Gobbini, M. Gnugnoli, M. Mangiagalli, M. Clerici, M. P. Longhese, Dpb4 promotes resection of DNA double-strand breaks and checkpoint activation by acting in two different protein complexes. *Nat. Commun.* **12**, 4750 (2021).
36. R. Bellelli, O. Belan, V. E. Pye, C. Clement, S. L. Maslen, J. M. Skehel, P. Cherepanov, G. Almouzni, S. J. Boulton, POLE3-POLE4 is a histone H3-H4 chaperone that maintains chromatin integrity during DNA replication. *Mol. Cell* **72**, 112–126.e5 (2018).
37. O. Z. Aydin, W. Vermeulen, H. Lans, ISWI chromatin remodeling complexes in the DNA damage response. *Cell Cycle* **13**, 3016–3025 (2014).
38. L. Lan, A. Ui, S. Nakajima, K. Hatakeyama, M. Hoshi, R. Watanabe, S. M. Janicki, H. Ogiwara, T. Kohno, S. Kanno, A. Yasui, The ACF1 complex is required for DNA double-strand break repair in human cells. *Mol. Cell* **40**, 976–987 (2010).
39. M. Hampsey, D. Reinberg, Tails of intrigue. *Cell* **113**, 429–432 (2003).
40. M. Gerber, A. Shilatifard, Transcriptional elongation by RNA polymerase II and histone methylation. *J. Biol. Chem.* **278**, 26303–26306 (2003).
41. M. B. Chandrasekharan, F. Huang, Z. W. Sun, Ubiquitination of histone H2B regulates chromatin dynamics by enhancing nucleosome stability. *Proc. Natl. Acad. Sci. U.S.A.* **106**, 16686–16691 (2009).
42. S. Sanchez-Molina, O. Mortusewicz, B. Bieber, S. Auer, M. Eckey, H. Leonhardt, A. A. Friedl, P. B. Becker, Role for hACF1 in the G2/M damage checkpoint. *Nucleic Acids Res.* **39**, 8445–8456 (2011).
43. F. J. Najm, P. DeWeirdt, M. M. Moore, S. M. Bevill, C. A. El Farran, K. A. Macias, M. Hegde, A. L. Waterbury, B. B. Liau, P. van Galen, J. G. Doench, B. E. Bernstein, Chromatin complex dependencies reveal targeting opportunities in leukemia. *Nat. Commun.* **14**, 448 (2023).
44. I. Vaicekauskaite, R. Sabaliauskaite, J. R. Lazutka, S. Jarmalaite, The emerging role of chromatin remodeling complexes in ovarian cancer. *Int. J. Mol. Sci.* **23**, 13670 (2022).
45. C. C. L. Chen, A. F. Andrade, N. Jabado, SMARCA4 vulnerability in H3K27M midline glioma: A silver bullet for a lethal disease. *Mol. Cell* **83**, 163–164 (2023).
46. S. Zhang, Y. Meng, L. Zhou, L. Qiu, H. Wang, D. Su, B. Zhang, K. M. Chan, J. Han, Targeting epigenetic regulators for inflammation: Mechanisms and intervention therapy. *MedComm (2020)* **3**, e173 (2022).
47. Y. Cheng, C. He, M. Wang, X. Ma, F. Mo, S. Yang, J. Han, X. Wei, Targeting epigenetic regulators for cancer therapy: Mechanisms and advances in clinical trials. *Signal Transduct. Target. Ther.* **4**, 62 (2019).
48. P. A. Jones, J. P. Issa, S. Baylin, Targeting the cancer epigenome for therapy. *Nat. Rev. Genet.* **17**, 630–641 (2016).
49. S. P. Jackson, J. Bartek, The DNA-damage response in human biology and disease. *Nature* **461**, 1071–1078 (2009).
50. A. Ciccia, S. J. Elledge, The DNA damage response: Making it safe to play with knives. *Mol. Cell* **40**, 179–204 (2010).
51. P. L. Olive, J. P. Banath, The comet assay: A method to measure DNA damage in individual cells. *Nat. Protoc.* **1**, 23–29 (2006).
52. J. Han, H. Zhang, H. Zhang, Z. Wang, H. Zhou, Z. Zhang, A Cul4 E3 ubiquitin ligase regulates histone hand-off during nucleosome assembly. *Cell* **155**, 817–829 (2013).
53. M. Wei, Y. Zhang, X. Yang, P. Ma, Y. Li, Y. Wu, X. Chen, X. Deng, T. Yang, X. Mao, L. Qiu, W. Meng, B. Zhang, Z. Wang, J. Han, Claudin-2 promotes colorectal cancer growth and metastasis by suppressing NDRG1 transcription. *Clin. Transl. Med.* **11**, e667 (2021).
54. X. Li, L. Liu, S. Yang, N. Song, X. Zhou, J. Gao, N. Yu, L. Shan, Q. Wang, J. Liang, C. Xuan, Y. Wang, Y. Shang, L. Shi, Histone demethylase KDM5B is a key regulator of genome stability. *Proc. Natl. Acad. Sci. U.S.A.* **111**, 7096–7101 (2014).

Acknowledgments: We are grateful to the core facility of State key Laboratory of Biotherapy and West China Hospital for the support and thank all financial supporters. We also thank L. Shi for NHEJ-EJ5 and DR-U2OS cell lines, J. Huang for plasmids and experimental advice, and Q. Xiong and Y. Zhang for technique support. **Funding:** This study was supported by grants from the National Natural Science Foundation of China (31972884), the Foundation for Innovative Research Groups of the National Natural Science Foundation of China (81821002), the National Key Research and Development Program of China (2022YFC1103702), the 1·3·5 Project for Disciplines of Excellence, and West China Hospital (ZYJC21021). **Author contributions:** Research design and conceptualization: X.M. and J.H.; experiment performing: X.M.; data analysis: X.M. and J.H.; figure creation: X.M. and S.Z.; material and technique support: J.W., S.Z., Q.Z., X.Li., X.C., X.W., L.Q., M.W., X.Le., M.Z., and C.L.; manuscript writing and revision: X. M. and J. H. **Competing interests:** The authors declare that they have no competing interests. **Data and materials availability:** All data needed to evaluate the conclusions in the paper are present in the paper and/or the Supplementary Materials.

Submitted 18 February 2023
Accepted 8 August 2023
Published 8 September 2023
10.1126/sciadv.adh2358